INVESTIGATION OF SEA WATER IN THE NORTH ATLANTIC OCEAN WITH A SHIPBOARD LIDAR

G.P. Kokhanenko, I.E. Penner, and V.S. Shamanaev

Institute of Atmospheric Optics,
Siberian Branch of the Russian Academy of Sciences, Tomsk
Received March 26, 1998

Long-term measurements of the extinction index of water were carried out with a shipboard lidar in the North Atlantic Ocean. Sensing was performed through the rough air-water interface. Three-week sensing at one geographical site has demonstrated that in case of changing water masses of different origin the dependence of the extinction index on the temperature of water has the form of a linear regression due to the activity of phytoplankton. Lidar measurements are compared with independent measurements of the depth of visibility of a standard white disc (Secchi disc). Some peculiarities of lidar return signals are discussed in case of shipboard lidar sensing of water. A method has been suggested to compensate for the effect of foam and surf caused by sailing ship on the accuracy of the lidar measurements.

The Makrel'–2 lidar developed at the IAO was placed on board the scientific vessel *Akademician Mstislav Keldysh* accomplishing the 37th mission organized by the Institute of Oceanology of the RAS. The fact that the lidar was specially designed for airborne measurements[1] was no barrier to its shipboard operation, though this imposed limitations on the experimental procedure. Shipboard lidars were also used by other scientific groups (see, for example, Refs. 2 and 3). However, they operated through a special trunk in the ship bottom and the effect of the rough sea surface was completely eliminated. In our case, there arised the unique situation. in which the scientific vessel drifted above one point (where the ship «Titanic» wrecked). This enabled us to measure purely temporal characteristics of water mass, which is rarely feasible. In addition, a number of spatiotemporal and methodical experiments were carried out in the course of three-week mission.

The lidar was placed in a cabin on the fifth deck. A laser beam was directed into water with an external mirror. The beam penetrated water at a distance of 4 m from the ship board near its center. The distance from the lidar to the point of laser beam penetrated into water was 18 m. The orientation of the mirror was adjusted to the polarization plane of laser radiation to minimize distortions of the polarization state of lidar return signals. The sizes of the mirror were larger than the aperture of lidar optics. In this series of measurements we used the lidar with the following parameters. The laser pulse duration at 532 nm was 12 ns (that is, the depth resolution in water was 1.8 m). The pulse energy was 30 mJ, and the maximum pulse repetition frequency was 25 Hz. As a rule, we operated at a pulse repetition frequency of 1 Hz. The angular beam divergence was 4 mrad. A telescope had a diameter of 0.14 m, a focal distance of 0.75 m, and a total field-of-view angle (FOVA) of 13 mrad.

Fairly large FOVAs were used for lidar sensing of water for a number of reasons connected with the rough air-water interface. In case of sensing of the atmospheric aerosol or cloudiness we used the minimum possible FOVA (equal to the laser beam divergence) to minimize the contribution of multiply scattered radiation and, hence, to ensure the maximum accuracy of reconstruction of the optical parameters of the medium. In case of sensing of water, the situation is different, because the laser beam is splitted randomly into many rays due to the sea surface roughness. The same is true for the laser beam coming from underwater that changes randomly its propagation direction. The increase on the angular beam divergence after the double passage of the beam through the air-water interface may cause the radiation of low scattering multiplicity to fall outside the lidar field of view. In this case, losses increase with the increasing depth.

Calculations performed by Kargin et al.[4] demonstrated that for small (of the order of 1 mrad) FOVAs the sea surface roughness caused not only the decrease of the average signal energy and, hence, of the maximum depth of sensing, but also significant overestimation of the rate of signal decay with the increase of the sensing depth and, hence, overestimation of the calculated extinction index. High-order scattering depends to a lesser degree on the state of sea roughness. The effect of the surface roughness decreases with the increase of the field-of-view angle.

0235-6880/98/07 614-07 $02.00

For FOVA ≥ 10 mrad, the rate of signal decay becomes less than that calculated for the plane air-water interface. For larger FOVAs, the process saturates. As a result, it is obvious that sensing of water with the minimum possible FOVA is inefficient. Another reason is that amplitudes of energy-carrying waves reach 1 m, that is, the distance to water in the object space of the receiving telescope changes from 17 to 19 m. In this case, the position of the image plane fluctuates by more than 3 mm, that is, not always coincide with the position of a lidar field stop. This leads to variable vignetting, which distorted the optical transfer function of the lidar; however, these distortions decrease for large diameter of the field stop of the telescope.

The above-indicated reasons led to significant fluctuations of the lidar signal power from pulse to pulse. The relative standard deviation of the amplitudes of lidar return signals was 30–35%. As a rule, the signal fluctuations remain unchanged when the depth of sensing increases; however, they decrease down to 25% for some series of sensing pulses.

One more peculiarity of lidar return signals is connected with glint reflections from micropatches perpendicular to the incident laser beam. We obtained empirically that to reduce glint reflections, the laser beam should be tilted at an angle of 13° to the vertical.

A signal from FEU–144 photomultipliers (recorded with a temporal resolution of 7 ns) was digitized with a 7-bit analog-to-digital converter (ADC). The data sampling period was 7.5 ns (which corresponded to a 0.84-m resolution in water). However, the dynamic range of the ADC (and of the photomultiplier) was insufficient for sensing of sea water from the sea surface to depths as great as 20–25 m. Therefore, calibrated light filters were inserted in the receiving channel in case of sensing at small depths. The attenuation coefficients of these filters were 5 and 27. To obtain the depth profile of lidar return signals, the measurements with different signal attenuation were averaged over 200 laser shots and then joined together in the region of their overlap. Typical waveforms of lidar returns obtained in such a way are shown in Fig. 1.

Serial numbers of signal counts and corresponding depth, in m, counted off from the water surface are plotted on the abscissa, and the lidar functions $S(h) = P(h)\,(H_0 + h/n)^2$ are plotted on the ordinate, where $m_0 = 18$ m is the distance to the sea surface, $n = 1.33$ is the refractive index of water, and $P(h)$ is the lidar signal power, in units of ADC code (bits). Curves *1…3* are for different values of water turbidity.

The maximum depth of sensing for the given values of attenuation of light fluxes is limited by the ADC quantization noise being equal to the ± 1 least significant bit. It changes from pulse to pulse. The average minimum and maximum depths at which we processed signals recorded with 5-fold attenuation are indicated by tilted arrows to the right of the curves. The noise level for lidar operation without filter is also shown in the figure by the dashed line. The error decreased down to ± 0.2 bit after averaging over 200 laser shots. As a rule, the maximum depth of sensing reached 25 m well offshore.

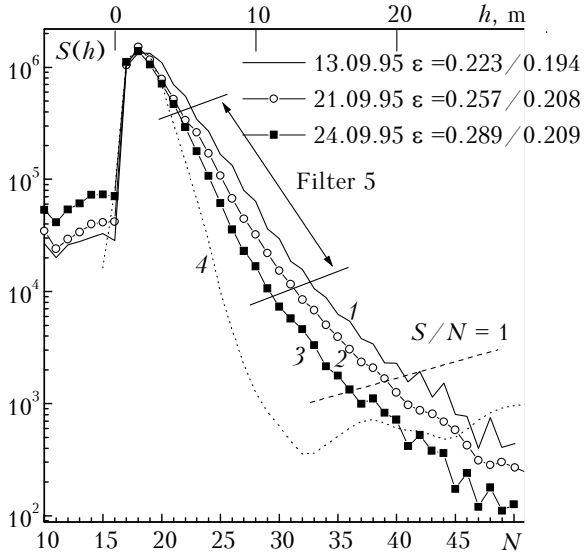

FIG. 1. Typical waveforms of lidar returns averaged over 200 laser shots. Here, N is the serial number of ADC counts and h is the depths in water.

To calculate the extinction index of water, we used the method of logarithmic derivative,[5] which is applicable for homogeneous optical characteristics of water. It should be noted that the place of wreck of *Titanic* is, from the viewpoint of oceanologs, «the oceanic desert». The water there has low bioproductivity and is oligotrophic. Therefore, its parameters vary only insignificantly. In this region we observed no spikes on lidar return signals caused by underwater inhomogeneities. Therefore, we succeeded in obtaining reliable average estimates of the extinction index of water from the rate of signal decay on logarithmic scale for the above indicated depths.

The minimum depth of sensing was chosen as the depth at which the signal amplitude was 90% of the maximum ADC amplitude in case of processing of a single pulse. The maximum depth of sensing was chosen as the depth at which the signal amplitude was 3 bits (the signal-to-noise ratio was equal to 3). The rate of signal decay between these two points was approximated with a straight line by the least squares technique and the extinction index was then calculated from the slope of this straight line. As indicated above, the minimum and maximum depths changed from pulse to pulse. The sensing range was 2.5–10 m for measurements with 27-fold attenuation, 4–13 m for measurements with 5-fold attenuation, and 8–20 m for measurements without filter. (Below we denote the extinction index calculated from these measurements as ε_{27}, ε_5, and ε_1, respectively.) Then the calculated values of ε were averaged over series of

measurements comprising, as a rule, 200 laser pulses. It took us 10 min to perform three successive series of measurements with different signal attenuation at pulse repetition frequency of 1 Hz. The parameters of water can be considered to be constant during measurement period. The correlation of the values of ε_{27}, ε_5, and ε_1 obtained for 3 weeks is shown in Fig. 2.

Here, ε_5 is taken to be an independent variable. The standard deviations for each run are also shown in the figure for ε_1 (the absolute error averaged over all runs was ± 0.014 m^{-1}, which made up 6% of the average value of ε_1). The regression has the form $\varepsilon_1 = (0.848 \pm 0.012)\ \varepsilon_5$ with the correlation coefficient $R = 0.87$. (The average absolute error in the estimable of ε_5 was ± 0.018 m^{-1}, which comprised 7% of the average value of ε_5).

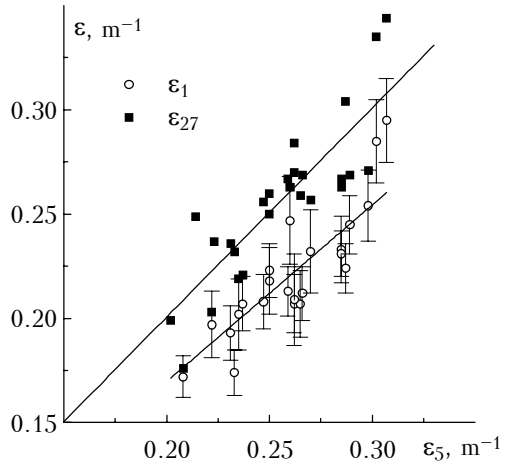

FIG. 2. Correlation of the values of the extinction index of water calculated from measurements with different light filters. The values of ε measured with 5-fold attenuation are plotted on the abscissa. Filled squares denote the values of ε measured with 27-fold attenuation. Open circles denote the values of ε measured without filter.

The average values of ε_{27} and ε_5 were practically identical ($\varepsilon_{27} = (1.003 \pm 0.014)\ \varepsilon_5$ with the correlation coefficient $R = 0.86$), whereas the spread of the values of ε_{27} was much greater (± 0.032 m^{-1}, which comprised 12% of its average value). This is explained by the fact that the inhomogeneous subsurface water layer (located at depth ≤ 3 m) was included when we processed the measurements with 27-fold signal attenuation. In this subsurface layer, signal waveforms may be distorted by the driving wind, and the glint reflections from the water surface also may affect the signal waveforms. Numerous air bubbles formed in this layer caused excess fluctuations of the extinction index of water.

It is difficult to explain the systematic underestimation of the values of ε_1 recorded by us for water layers at greater depths. Already in Fig. 1 a noticeable decrease of the slope of curves can be seen at depths as great as 12–15 m. (Here, the values of ε shown through the solidus at the top of the figure were calculated for the initial and end segments of the curves). Such behavior was typical of most signals measured by us during the mission. In the present paper, we give only some considerations to possible reasons for such behavior of signals.

1. It is possible that in some cases the extinction index decreased really with the increase of depth. This is consistent with the data of regular observations[5] and may be caused not only by the peculiarities of depth behavior of phyto- and zooplankton, but also by the effect of subsurface air bubbles and foam.

2. As pointed out above, the wind-driven sea waves cause faster decay of singly scattered radiation with the increase of the depth. At the same time, multiply scattered radiation is the dominant component at great depths. It causes the apparent underestimation of the refractive index. The combined effect depends on the state of sea roughness and hitherto eludes simple estimation. We can only conclude that the effect of surface roughness was no longer observed by us at depths greater than 12 m (during our observations, the driving wind velocity was < 10 m/s).

3. We investigated the effect of the finite pulse length on the data of lidar sensing. The matter is that the pulse length in our experiments was only several times less than the extinction length ($1/\varepsilon$) in the scattering medium. The waveform of lidar signal reflected from a flat interface is shown by the dashed curve (curve *4*) in Fig. 1. It can be considered as the lidar pulse response $K(h)$, which takes into account not only the form of a laser pulse, but also the temporal resolution of the receiving aperture (photomultiplier + ADC). A lidar return signal $P(h)$ recorded experimentally is a convolution of the function $K(h)$ with the pulse response of the water medium $P_\delta(h)$ to a short light δ-pulse

$$P(h) = \int_0^h K(h - r)\ P_\delta(r)\ \mathrm{d}r.$$

It is precisely the function $P_\delta(h)$ that is really described by the laser sensing equation. When the form of the function $K(h)$ is known, we can use regularization algorithms[6] to solve the convolution equation and to reconstruct the nondistorted pulse response $P_\delta(h)$. Numerical modeling showed that significant distortion of lidar return signal due to the finite lidar temporal resolution occurs only in the turbid medium with the extinction index $\varepsilon > 0.55$ m^{-1}. In our case ($\varepsilon < 0.35$ m^{-1}), the difference between the values of the extinction index calculated from true lidar return signals and from the reconstructed pulse response was within the limits of the total measurement error. However, the possibility of nonlinear variations of the temporal response of the photomultiplier must not be intense out in case of the

intense background illumination. This makes the convolution equation inapplicable for the description of lidar return signals. This problem calls for further investigations.

The experimental site *Titanic* is characterized by the warm Gulfstream flowing to the north side by side with the cold Labrador-stream flowing to the south (one of the phenomena of Bermudan triangle). Sometimes this leads to the fast change of the water mass type (and, hence, of water temperature) even on the sea surface. This also lead to the change of water turbidity, because the content of oxygen in water increases with the decrease of its temperature thereby accelerating the growth of phytoplankton and microorganisms (that is, hydrosols). Figure 3*a* shows the correlation between the temperature of water and its extinction index ε_1 for 22-day period. The regression has the form $\varepsilon_1 = 0.368 - 0.0095\,T$ with the correlation coefficient $R = -0.83$. Figure 3*b* illustrates the most vivid manifestation of this dependence obtained on September 24, when the water temperature decreased by 5° for 8 h (the temperature of water measured by a submerged temperature gauge at a depth of 50 m reached − 1°q).

The standard deviation for each run of ε_{27} is shown in Fig. 3*b*. It was between 11–14 %. In this special case, the regression has the form $\varepsilon_{27} = 0.434 - 0.014\,T$ with the correlation coefficient $R = -0.934$ for the range of temperatures $T = 10$–16°q . We should focus our attention on the fact that the correlation of $\varepsilon(T)$ demonstrates that the variations of the water turbidity factor at this experimental site are caused by the change and mixing of water masses of two types (of the Labrador- and Gulf-streams) having different temperatures and turbidity factors. In other cases, in which the temperature variations are caused, for example, by water heating, the form of the dependence $\varepsilon(T)$ can differ or it can vanish at all, because there are some other reasons for water turbidity variations. Nevertheless, our measurements demonstrated the feasibility of reliable identification of the change of water transparency connected with the bioproductivity of water in the examined case.

The degree of homogeneity of water can be inferred by Fig. 4 which displays a set of lidar signals corresponding to Fig. 3*a*. Here, a set of 1500 lidar return signals averaged over 10 laser shots, that is, over 10 s, is displayed on scale of gray versus the temperature of water. The contour lines of lidar signal power have the clearly pronounced tendency for the increase of their depths with the increase of the surface water temperature. However, spikes on the contour lines whose amplitude exceeded the noise level testify to the occurrence of a certain fine internal structure. It should be noted that inhomogeneous water structure was qualitatively detected (without measuring the extinction index) earlier in Ref. 3.

Up to now, much attention is given to the relation between the depth of visibility of a standard white disc (Secchi disc) Z_d and the extinction index of water ε. This interest is primarily caused by the simplicity of measuring Z_d and the fact that large databank of this parameter is available for all oceans. True, these measurements can be performed only in the daytime when sea surface roughness is small and the ship does not move. The generally accepted relation has the form[7] $\varepsilon Z_d = a$. The parameter a of this regression relation changes in a wide range from 3.5 to 7.7 in most situations. This wide range of variations is due to a wide range of variations of hydrosol composition and hence of hydrosol scattering phase function. It is the scattering phase function that determines primarily the masking effect of the solar radiation scattered in the water column on visual observations of the white disc.

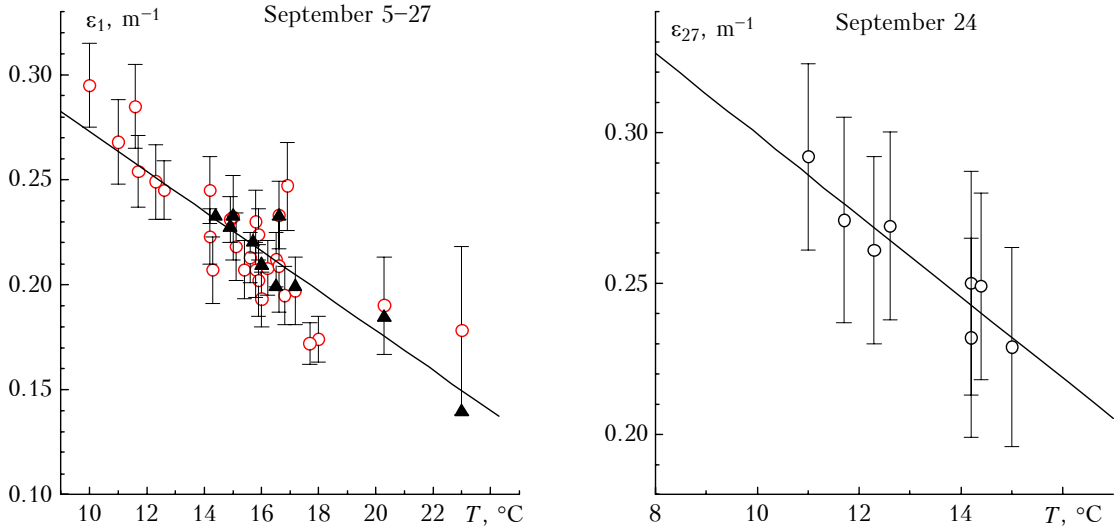

FIG. 3. Dependence of the extinction index on the temperature of water caused by the change of water mass type at the point of drifting ship. Here, triangles denote the values of ε *calculated from the depth of visibility of the Secchi disc.*

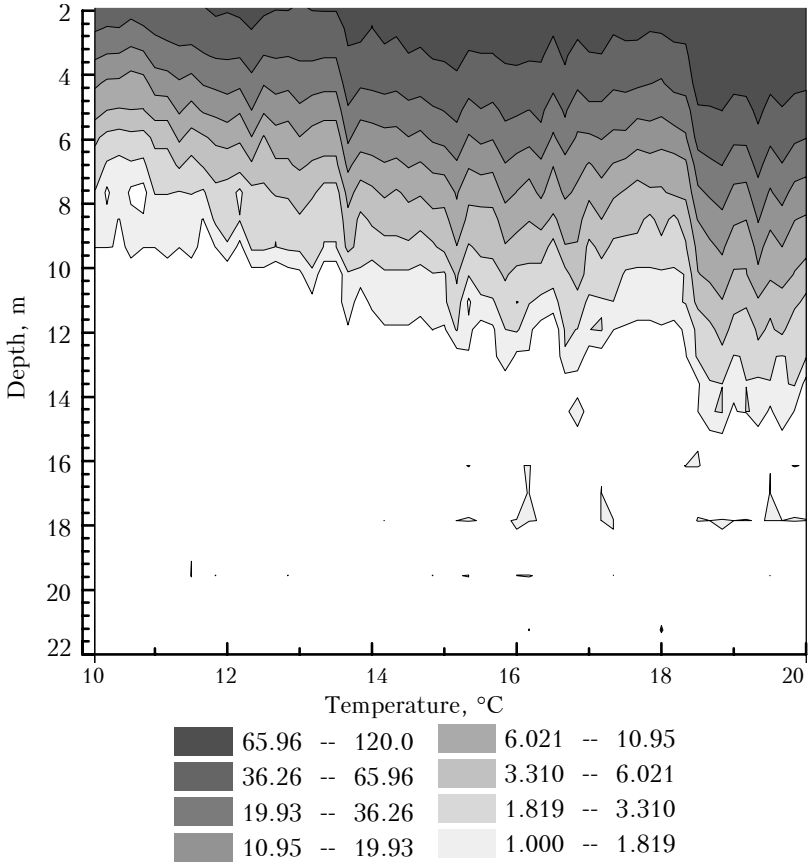

FIG. 4. Lidar return signals at different temperatures of water. The scale of gray, in ADC bits, is shown at the bottom of the figure for signals averaged over 10 laser shots.

In this experiment, the visibility depth of the Secchi disc was measured by the scientists of the Institute of Oceanology of the RAS. The data were kindly provided to us by V.N. Artem'ev. Unfortunately, these measurements were not synchronized with lidar ones and the time delay reached several hours. Indirect comparison of all lidar measurements of ε_1 and measurements of Z_d performed on September 5–27 considering the dependence of water turbidity on the temperature is shown in Fig. 3*a* in which filled triangles are for $\varepsilon_d = a/Z_d$ with $a = 4.2$. The regression has the form $\varepsilon_d = 0.363 - 0.0098\,T$ with the correlation coefficient $R = 0.939$. The slope of the regression straight line deviates only by 3% from that of the dependence $\varepsilon_1(T)$. The best suited value of the parameter a is $a = 4.75$ if we compare ε_{27} and Z_d.

Direct comparison with lidar-derived data is illustrated by Fig. 5 for measurements on 09.14.95 when the water temperature decreased with time. The values of the extinction index of diffuse radiation in water K_d measured at 490 nm with the Al'famer–21 measuring device,[5] developed at the Institute of Oceanology are also shown in this figure. The lack of one-to-one correspondence between the data can be vividly seen. The dependence $Z_d(\varepsilon)$ is best fitted by the relation $Z_d = a/\varepsilon$ with $a = 5.5$. This value of the parameter a is within the above-indicated range of variations of this parameter.

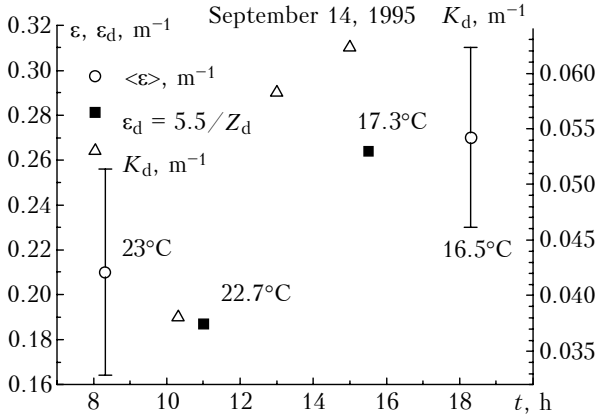

FIG. 5. Comparison of lidar-derived extinction index ε (circles) with the extinction index ε_d calculated from the visibility depth of the Secchi disc (filled squares) and the extinction index K_d for the diffuse radiation (triangles).

As already mentioned above, the lidar was placed at the center of the ship. Unpleasant consequences of such location of the lidar were foam and splash of water that appeared when the ship sailed with the

velocity > 2 m/s and fell into the lidar field-of-view angle. In this case, the signal reflected from the sea surface increased significantly, because the foam albedo was high and its scattering phase function was wide. The signal coming from the sea surface may even mask the hydrosol component of lidar return signals coming from great depths. The rate of subsurface signal decay in the trailing edge of the pulse increased and therefore we obtained overestimated values of ε from the formula of the logarithmic derivative.

Figure 6 shows a comparison of the data obtained on 09.21.95 from a board of the drifting ship (the velocity of the ship was $v = 0$) and when the ship sailed ($v = 4.2$ m/s) back to the measurement site after it had been carried by the Gulfstream. Figure 6*a* shows the histogram of distribution of the lidar return signal energy, in relative units, measured with 5-fold signal attenuation. The values of energy E plotted on the abscissa were calculated by integration of the entire lidar return signal between the noise limits under the same conditions of sensing. The number of pulses having the preset value of the energy $n(E)$ in a series of 200 laser shots is plotted on the ordinate, that is, this figure illustrates the empirical probability density of occurrence of the given values of the energy e, in relative units. It can be clearly seen that nearly Gaussian initial distribution $n(E)$ is extended to the right, thereby indicating significant number of lidar return signals with increased energy caused by reflections from foam and surf.

The histogram of the recurrence of calculated values of ε is shown in Fig. 6*b*. It also can be seen from the figure that the initial symmetric distribution $n(\varepsilon)$ is deformed. It broadens toward larger values of ε. Because the signals with large energy correspond to the reflections from foam, only weak lidar return signals (with small energy), penetrating water through foam-free sections of the sea surface, carry information about the true values of the extinction index. This provides a basis for a simple and efficient procedure of elimination of the distorting effect of foam.

If in a long series of laser shots we exclude from consideration the signals with energy larger than its average value $\langle E \rangle$ for the examined distribution $n(E)$ (for Fig. 6*a*, $\langle E \rangle = 375$ rel. units), the value of ε estimated from the remaining signals will be much less distorted by surface reflections. The distribution of the extinction index in this case is illustrated by Fig. 6*c*. It is well approximated by the normal distribution. The difference between $\varepsilon = 0.253 \pm 0.039$ m^{-1} derived for sailing ship and $\varepsilon = 0.246 \pm 0.020$ m^{-1} calculated for drifting ship is less than the width of the distribution. (When we processed all signals in that run, we obtained $\varepsilon = 0.287 \pm 0.066$ m^{-1}).

The efficiency of the procedure of rejection of signals burdened with the interaction with foam is well seen from the data of sensing on 10.09.95, when the ship sailed with a velocity of 6.4 m/s and the sea surface near the ship was mostly covered with foam (Fig. 7).

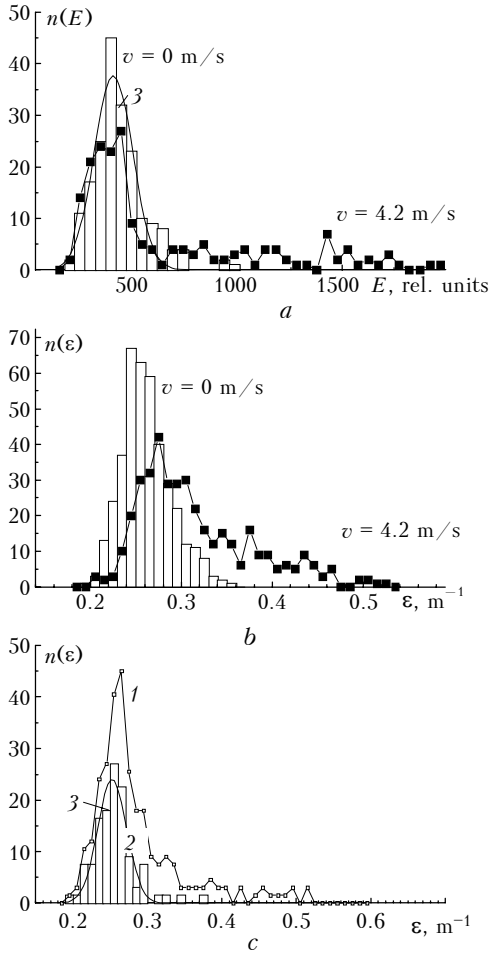

FIG. 6. Comparison between the data obtained from a board of the drifting ship and when the ship sailed with a velocity of 4.2 m/s: *distributions of the lidar return signal energy (a), calculated extinction index (b), and the extinction index measured when the ship sailed (c) calculated for the entire data array (1) and for lidar return signals with energy less than its average value (2). Curve 3 shows the Gaussian approximation.*

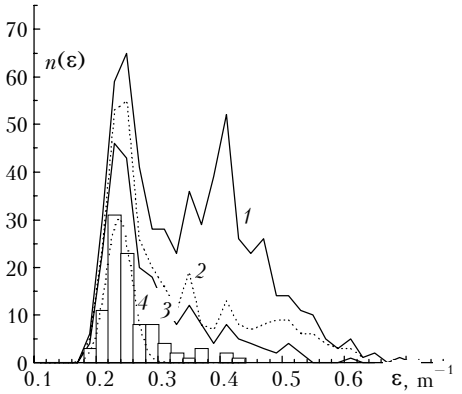

FIG. 7. Change of the form of the extinction index distribution calculated for the sailing ship with successive rejection of lidar return signals with energy exceeding the preset threshold.

Actually, the value of ε averaged 600 laser shots was $\varepsilon = 0.355 \pm 0.106$ m^{-1}. The distribution $n(\varepsilon)$ shown by curve *1* is bimodal in character. Rejecting successively the pulses with energy larger than 1.1, 0.93, and 0.8 of its average value (curves *2–4*) from the initial array of laser return signals, we see that the second mode of the distribution vanishes. The last distribution (curve *4*) is well approximated by the Gaussian distribution with $\varepsilon = 0.237 \pm 0.021$ m^{-1}, which can be considered as a reliable estimate of the extinction index.

The results obtained at different times for sailing ship are summarized in Table I. In September, 200 laser shots were processed, and 600 shots were processed in October. The time at which the measurements started is given in the second column. The fourth column gives the surface water temperature, the fifth column gives the velocity of ship v, and the sixth column gives the driving wind velocity w. The driving wind velocity and the surface water temperature were measured with a shipboard meteorological station. The values of the extinction index ε_{27} and ε_5 were obtained using the above-described experimental procedures. Dashes in the columns giving the corresponding values of variance $\pm\sigma$ signify data omissions in cases in which the histogram could not be approximated by the Gaussian distribution due to large number large values of ε; in these cases the modal value of ε is given in the Table. The extinction index measured without filter ε_1, as a rule, was independent of the signal energy, because it corresponded to signals coming from greater depths and was much less affected by the state of surface roughness. In that case we simply averaged the value of ε over a series of measurements.

TABLE I. Measurements of the extinction index of laser radiation by water of the North Atlantic Ocean.

Data	Time	Coordinates	T, °C	v, m/s	w, m/s	ε_{27}, m^{-1}	$\pm\sigma_{27}$, m^{-1}	ε_5, m^{-1}	$\pm\sigma_5$, m^{-1}	ε_1, m^{-1}	$\pm\sigma_1$, m^{-1}
6.09	20:23	42°34′N, 54°44′W	21.2	5.4	3.0	0.31	0.062	–	–	0.19	0.015
11.09	18:28	40°26′, 49°12′	25.0	3.7	6.0	0.21	–	–	–	0.15	0.014
16.09	16:01	41°44′, 49°57′	16.4	3.7	12.0	0.35	0.045	0.26	0.028	0.21	0.022
21.09	16:22	41°44′, 49°55′	15.2	4.2	6.9	0.29	0.036	0.25	0.019	–	–
9.10	20:47	48°05′, 22°20′	16.4	6.4	7.3	0.31	0.065	0.23	0.021	–	–
10.10	20:53	48°49′, 15°05′	16.2	6.2	15.8	–	–	0.27	–	0.24	–
11.10	20:48	49°27′, 07°28′	15.7	6.7	8.6	–	–	0.39	0.033	0.35	–
12.10	12:48	49°52′, 02°34′	14.9	6.4	0.9	–	–	0.27	0.024	0.25	0.017
12.10	18:36	50°12′, 00°56′	16.6	6.7	0.7	–	–	0.37	0.029	–	–
12.10	20:41	50°20′, 00°14′	16.8	6.9	1.9	–	–	0.41	0.035	0.39	0.031

Of interest are the measurements carried out on 09.11.95 at the experimental site *Titanic* when the surface water temperature was 25°q (maximum for the period of observations). The estimated values of ε_{27} and ε_1 were minimum (see Fig. 3*a*, from which $\varepsilon_1 = 0.14 \pm 0.03$ m^{-1} was predicted at $T = 24$°q). This value of ε_1 deviated from the measured one by no more than the rms error. As expected (see two last rows at the bottom of the Table), the water turbidity increased markedly when the ship sailed through the English Channel.

Thus, we can conclude the following. Our measurements have shown the feasibility of measuring the extinction index of water ε with a shipboard lidar through the air-water interface (without special trunk) irrespective of the time of a day under conditions of a strong wind. Shipboard observations call for significant statistics due to the occurrence of foam and surf in the zone of lidar operation (the optimal position of lidar in this case would be on the forward deck of a ship). The values of the extinction index measured for homogeneous water at different depths with different signal attenuation factors are well correlated. The small bias of the estimates in this case was caused by the effect of multiple scattering and wind-driven sea waves. The lidar measurements agree well with the independent measurements of the visibility depth Z_d of a standard white disc. The relation between ε and Z_d is consistent with the data published in the literature.

ACKNOWLEDGMENT

We are grateful to M.M. Krekova for useful discussion of the results of our observations and analysis of the effect of wind-driven sea waves on lidar signal waveforms.

REFERENCES

1. A.I. Abramochkin, V.V. Zanin, I.E. Penner, et al., Opt. Atm. **1**, No 2, 92–96 (1988).
2. Yu.A. Gol'din and M.A. Evdoshenko, Oceanology **26**, No. 5, 761–762 (1986).
3. O.A. Bukin, V.I. Il'ichev, A.Yu. Maier, et al., Atmos. Oceanic Optics **7**, No 10, 761–763 (1994).
4. B.A. Kargin, G.M. Krekov, and M.M. Krekova, Atmos. Oceanic Optics **5**, No 3, 191–195 (1992).
5. A.S. Monin, ed., *Oceanic Optics.* V. 1. *Physical Optics of the Ocean* (Nauka, Moscow, 1983), 372 pp.
6. A.N. Tikhonov, A.V. Goncharskii, et al., *Regularizing Algorithms and a priori Information* (Nauka, Moscow, 1983), 200 pp.
7. O.A. Sokolov, *Underwater Visibility* (Gidrometeoizdat, Leningrad, 1974), 232 pp.